PROCEEDINGS OF SCIENCE

Pulsar High-Energy Emission Models

Alice K. Harding[a,*]

[a] *Los Alamos National Ladoratory, Los Alamos, NM 87545, USA*

E-mail: ahardingx@yahoo.com

Ground-based Air-Cherenkov telescopes have detected pulsations at energies above 50 GeV from a growing number of *Fermi* pulsars. These include the Crab, Vela, PSR B1706-44 and Geminga, with the first two having pulsed detections above 1 TeV. There appears to be Very-High-Energy (VHE) emission that is an extension of the *Fermi* spectra to high energies as well as additional higher-energy components that require a separate emission mechanism. A variety of models for emission from rotation-powered pulsars at gamma-ray energies invoke different combinations of mechanisms. They also assume different emission locations in the magnetosphere including outer gaps, extended slot gaps and the current sheet outside the light cylinder. I will review the most recent models for VHE emission in light of the present data and their predictions for observations by existing and future telescopes.

*** *High Energy Astrophysics in Southern Africa (HEASA2021)* ***
*** *13 - 17 September, 2021* ***
*** *Online* ***

*Speaker

PoS(HEASA2021)047

1. Introduction

The past ten years has seen a dramatic revolution in our understanding of rotation-powered pulsars, both from vast improvements in observational capability and from major theoretical developments. The *Fermi* Large Area Telescope (LAT) has produced a stunning increase in the number of pulsar detections at GeV energy (253 at present) as well as a huge improvement in quality of data. In the first year of operation alone, *Fermi* observations of the Vela pulsar [1] were able to rule out polar cap models (emission at low altitudes), confirm the first pulsed γ-ray emission from millisecond pulsars [2] and discover a new class of radio-quiet γ-ray pulsars [3]. Shortly after, MAGIC announced the detection of pulsed emission from the Crab pulsar at energies up to $\sim$ 25 GeV [4], making this the first detection of a pulsar with a ground-based Cherenkov telescope. This was followed by the VERITAS detection of pulsed photons from the Crab up to $\sim$ 400 GeV [5], and finally, MAGIC detected pulsations up to 1.5 TeV [6]. The H.E.S.S.-II telescope then detected pulsed emission from the Vela pulsar in the sub-20 GeV to 100 GeV range [7]. They also reported pulsed emission from this pulsar at a few TeV (H.E.S.S. Collaboration, in preparation). More ground-based gamma-ray detections of pulsars quickly followed with H.E.S.S.-II reporting pulsed emission from PSR B1706−44 up to 70 GeV [8] and MAGIC reporting of pulsed emission from the Geminga pulsar between 15 GeV and 75 GeV [9]. The measured spectra in the sub-100 GeV range for Vela, B1706−44 and Geminga seem to smoothly connect to the spectra measured by *Fermi* LAT, so it is not clear whether this emission requires a separate spectral component. Also in all three cases, only the second light curve peak is visible, extending the trend of disappearing first peaks with increasing energy observed by *Fermi* to these higher energies.

2. Emission Models

Models for high-energy emission have evolved significantly over the years since GeV pulsations from the Crab and Vela were first detected in the 1970s, with the proposed location of the observed radiation initially close to the neutron star at the polar caps and gradually moving outward to near the light cylinder, $R_{\rm LC} = \Omega/c$ where Ω is the pulsar rotation rate and c is the speed of light, and most recently to the current sheet outside $R_{\rm LC}$ (see Figure 1). As mentioned above, polar cap models for the high-energy emission have been ruled out by *Fermi*, I will discuss only the high-altitude models here although particle acceleration and pair cascades are thought to be operating above the polar caps.

2.1 Slot Gap and Annular Gap

The outer rim of the polar cap borders the closed magnetic field region which is assumed to be force-free (FF) and fully conducting, forcing the electric field parallel to the magnetic field, $E_\parallel$, to zero. The slot gap (SG) is a narrow set of field lines near this boundary in which particles accelerate more slowly and never radiate photons with high-enough energy to produce pairs before the magnetic field drops too low. In the SG, the $E_\parallel$ is never screened by pairs and particle acceleration and radiation continue up to high altitude [10]. High-energy emission can thus be produced over a large range of radii from the neutron star surface to near the light cylinder [11]. Along trailing field lines, the observed phase differences of radiation due to the curved field is canceled by aberration

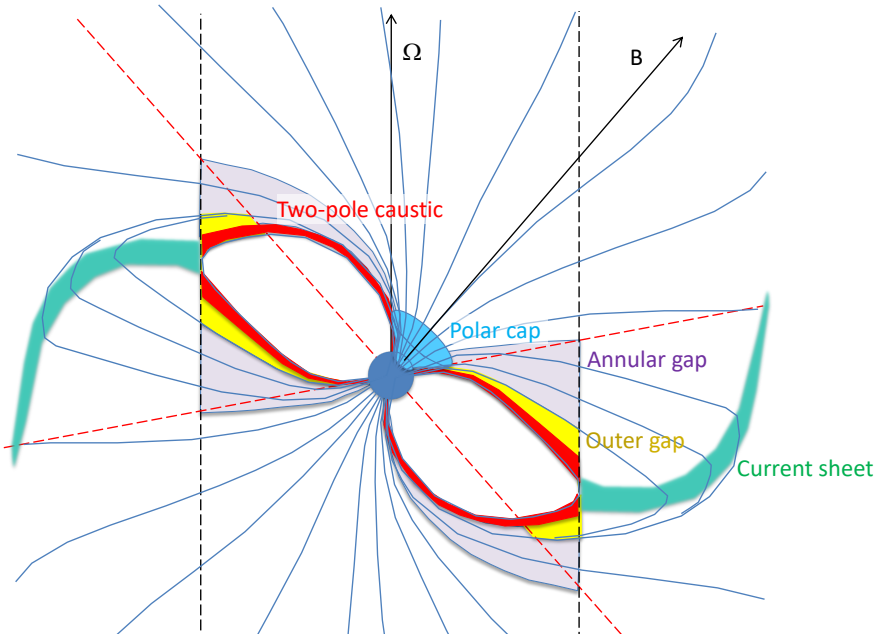

Figure 1: Location of polar cap/radio (blue) and high-energy emission in the outer gap (yellow), two-pole caustic (red), annular gap (purple) and current sheet (green) models in the meridional plane containing the spin and magnetic axes of a near force-free magnetosphere. The dashed black lines denote the light cylinder and the dotted red lines show projections of the null-charge surface.

and light travel time delays, forming caustics so that all the radiation arrives to the observer in phase. In such a two-pole caustic model (TPC, [12]) caustic patterns from both magnetic poles form one or two peaks with variable spacing in the light curves. The slot gap produces light curves like those of the TPC model, with varied separation of peaks for different observer angles that have phase lags with respect to the radio peaks [13], similar to those of *Fermi* pulsars.

The annular gap model is geometrically similar to the slot gap with two concentric regions of the polar cap: the annular field lines are those that cross the null charge surface within the light cylinder and are located at the outer edge of the polar cap while the core field lines are those interior to the annular gap [14]. Unlike the outer gap, the annular gap model assumes that the magnetosphere is not charge-separated but consists of a quasi-neutral pair plasma. In the core region, the $E_\parallel$ is screened at a low altitude by pairs since the local charge density ρ has the same sign as $\rho_{\rm GJ}$, but in the annular gap the pairs do not screen the $E_\parallel$ since ρ has the opposite sign as the Goldreich-Julian charge density, $\rho_{\rm GJ} = -\Omega \cdot B/(2\pi c)$ [15] and acceleration can continue to high altitude. The caustics of the γ-ray light curves from annular gaps are similar to those of the slot gap and can also fit many of the *Fermi* pulsar light curves. An annular gap model for the Crab pulsar [14] accounts for the *Fermi* emission as a blend of synchrotron radiation (SR) and curvature radiation (CR) from primary accelerated particles and the MAGIC spectrum as synchrotron self-Compton (SSC) from pairs.

2.2 Outer Gap

In a charge-separated magnetosphere, vacuum gaps can develop between the null charge line where $\rho_{\rm GJ}$ changes sign and the light cylinder, if particles of one sign flow out along open field lines but there are no charges below to replace them [16]. Outer gaps (OGs) also require that there be no polar cap pair cascades that send a super-Goldreich-Julian particle flux into the gap. The gap accelerates primary charges to produce CR, but at higher altitude above the neutron star pairs are created by the photon-photon process, using thermal X-rays from the neutron star surface, since the field is too low for magnetic pair production. The 3D geometry of the outer gap was modeled by [17], using the retarded vacuum dipole magnetic field [18] and emission up to but inside the light cylinder, producing γ-ray light curves with one or two peaks from the same rotational hemisphere. More recent models of the global pulsar magnetosphere (see Section 2.3) indicate that the Goldreich-Julian charge distribution required by FF magnetospheres does not contain regions of a single sign of charge since pair production populates most field field lines with both electrons and positrons, thus questioning the existence of outer gaps (see Section 2.3).

2.3 Current Sheet

The first solution to the global FF magnetosphere [19], the solution of Maxwell's Equations for a rotating star with a dipole field, ignoring plasma pressure and requiring that the electric field parallel to the magnetic field is zero everywhere ($\mathbf{E}\cdot\mathbf{B}=0$), showed that a current sheet forms outside the light cylinder. In this special case (FF and ideal MHD), the charge density in the magnetosphere is equal to the Goldreich-Julian charge density, $\rho_{\rm GJ}$, which is the density required to locally screen the $E_\parallel$. The current sheets are locations of dissipation, most likely from reconnection, as the magnetic field lines from the two poles having opposite polarity come together. If the FF condition is relaxed, dissipative magnetosphere solutions can be found for different values of a macroscopic conductivity σ [20, 21]. The dissipative global magneto-hydrodynamic (MHD) models show that the regions of acceleration do lie mostly outside the light cylinder near the current sheet. Using global models with infinite conductivity σ (FF) inside the light cylinder and finite σ outside the light cylinder and assuming that the accelerated particles radiate CR at GeV energies, [22] found that the predicted particle acceleration and radiation patterns matched the characteristics of the *Fermi* pulsars. Most recently, particle-in-cell (PIC) kinetic models have been used to fully compute the self-consistent feedback between particle motions and fields by injecting pairs or simulating pair production in the magnetosphere [23, 24]. For increasing pair injection rates that approach FF conditions, the $E_\parallel$ is screened over a large part of the magnetosphere and confined to the current sheet, where the highest energy particles are found. PIC simulations that include the General Relativistic frame-dragging effect on $\rho_{\rm GJ}$ have shown that pairs can be produced over larger regions of the magnetosphere [25]. A recent simulation of an axisymmetric pulsar magnetosphere with self-consistent pair production and very high resolution found that neither a charge-separated flow nor dissipation occurs near the region of the null charge surface, raising doubts about the formation of outer gaps [26].

3. Pulsar Spectral Models

3.1 Crab

Early OG models for the Crab [27] predicted that the observed GeV emission is a blend of SR at lower energies and ICS at higher energies, all from pairs produced by gap cascades. Later OG models [28] predicted an additional ICS component up to 10 TeV energies at a level that depends on the infra-red (IR) photon flux and enough absorption by γ-γ pair production not to exceed the upper limits from the current telescopes. Improved 3D OG models [29] modeled the Crab spectrum with SR from pairs to explain the optical through hard X-rays, and a combination of ICS and CR from primaries to explain the GeV emission. An OG model for the Crab spectrum including the MAGIC and VERITAS data up to 100 GeV was presented by [30], in which the emission below 10 MeV is dominated by SR from secondary pairs, the emission between 10 MeV and 25 GeV is dominated by CR from primaries and that between 25 GeV and 180 GeV is dominated by SSC from secondary and tertiary pairs. [31] proposed an OG model for the Crab where the spectrum below $\sim$ 100 MeV is produced by SR from pairs but the high-energy emission accounting for *Fermi* and MAGIC points is produced by cyclotron self-Compton of pairs. This model requires very high pair multiplicity of $\sim 10^6$ which may not be possible from the OG alone.

An SG model for the Crab phase-averaged and phase-resolved spectra was presented by [13] using the vacuum retarded dipole field structure. Similar to the OG models, the optical through X-ray spectrum is explained by SR of pairs that in SG models are produced by cascades at the polar caps and that acquire pitch angle through cyclotron resonant absorption of radio photons. The spectrum above 200 MeV is produced by a combination of SR and CR of primaries. This model however could not account for the MAGIC spectrum up to 25 GeV nor the later-detected VERITAS and MAGIC emission at higher energies. An annular gap model for the Crab phase-averaged and phase-resolved spectra was presented by [14], explaining the optical through hard X-ray spectrum by pair SR and the *Fermi* spectrum by a combination of SR and CR from primaries, as in the SG model. However, they introduced an additional component of ICS from pairs to explain the MAGIC and VERITAS points.

A model for the Crab high-energy emission from ICS of optical and X-ray photons in a cold wind was proposed by [32]. The ICS spectrum however cuts of around 500 GeV and cannot account for the pulsed emission later detected up to 2 TeV. [33] presented a similar wind model in which SR produces the emission up to $\sim$ 100 GeV and an ICS component produces a spectrum that cuts of around 10 TeV, invoking Doppler boosting of the emission by the wind bulk flow. [34] introduced a model for the Crab spectrum using an FF magnetosphere structure in which particles are assumed to be accelerated from the neutron star surface near the polar cap rim up to and beyond the light cylinder into the current sheet. Pairs from the polar caps flow on field lines just inside the SG and into the current sheet, resonantly absorbing radio photons to gain pitch angles and radiate SR, as in [13]. This model included additional ICS components from pairs (SSC), that can account for the MAGIC and VERITAS data, and primaries scattering the pair SR, that predicts a component above 1 TeV. Although, this model did not cover the energy range above $\sim$ 3 TeV, by extending the modeled energy range up to 100 TeV and including absorption by two-photon pair production, [35] showed that the primary ICS component extends beyond 10 TeV where it displays a sharp cutoff at 30 TeV, the maximum energy of the accelerated particles.

3.2 Vela

The early OG models [27] proposed that the Vela GeV emission is entirely SR from pairs and also predicted an ICS component from these same particles at energies up to several TeV with 10^{-2} of the power radiated in the GeV spectrum. Such an ICS component at TeV energy was also predicted by [36] at the same power level, where in this model the GeV emission is now CR. The rapid improvement of TeV telescopes soon after ruled out such a high level of ICS emission. However, the much lower flux of IR emission for Vela makes the prospect of using γ-γ absorption to reduce the predicted TeV flux more difficult. Later OG models (e.g. [37]) extended the previous 1D and 2D two-layer gaps to 3D and presented improved studies of Vela spectra and light curves with CR of primaries at GeV energy. They were able to produce the third Vela light curve peak whose phase moves with energy.

A current sheet model for Vela discussed by [33] produces the GeV emission by SR, extending out to 100 GeV using Doppler boosting of the photons by the bulk wind flow. However, the SSC component at higher energies is lower by several orders of magnitude compared to their Crab model SSC. An alternative current sheet model by [34] models the GeV emission as CR. An update of this model [38], extending the modeled energies beyond 10 TeV, predicts an ICS component from primaries scattering lower altitude SR from pairs that may be detectable by H.E.S.S.-II. The spectrum has a sharp cutoff around 30 TeV at the maximum particle energy. Thus, a detection of this component and the measurement of the cutoff would provide a lower limit on the particle energy. The model update (see also [35]) included a hybrid acceleration with lower $E_{\parallel}$ inside $R_{\rm LC}$ and a higher value in the current sheet. The detection of pulsed emission by H.E.S.S.-II between 10 and 100 GeV is modeled as the high-energy extended tail of the CR spectrum. The observed harder spectrum for the second light curve peak naturally follows from the higher radius of curvature of the trajectories of the particles producing the CR emission (see also [39]). The VHE emission detected by MAGIC from Geminga and by H.E.S.S.-II from PSR B1706-44 can also be modeled as the high-energy tail of primary CR emission [35].

4. Outstanding Questions

There have been many recent advances in detection and modeling of VHE emission from pulsars, with a significant number of *Fermi* pulsars with the highest γ-ray fluxes having been detected at energies above 50 GeV, with indications of pulsed emission above 1 TeV from the Crab and Vela. All recent global models strongly point to the current sheet as the site of most high-energy particle acceleration and radiation. However, these models disagree both on the source of the radiating high-energy particles and on the mechanism of the GeV emission. Some studies have suggested that most of the GeV and VHE-radiating particles are pairs produced at the Y-point and current sheet [24] while other studies suggest that the high-energy particles can come from near the neutron star [35, 40]. If polar cap cascades at the base of the separatrix can produce enough pairs, then some of these particles will flow into the current sheet and be accelerated to high energy. However, the PIC models are still in their infancy and will require some major advancements in order to provide realistic predictions for pulsar emission. Currently there is an enormous disparity of scales between what is needed for the global models and for the pair cascade microphysics. The

energy range that is possible in PIC models is also orders of magnitude smaller than in real pulsars. These problems may eventually be addressed by a combination of increased computational power and hybrid (MHD/PIC) modeling.

Some current models claim that the GeV emission is produced by SR emitted by particles accelerated to Lorentz factors of $\sim 10^5 - 10^6$ by reconnection in the current sheet [24, 41]. Others suggest that the GeV emission is CR produced by particles of much higher Lorentz factors $\sim 10^7 - 10^8$ in radiation-reaction limit in the current sheet [23]. Yet other studies [42] suggest that the GeV emission is ICS produced by pairs in the OGs. [43] have shown that *Fermi* pulsars lie on a fundamental plane in surface magnetic field, spin-down power, γ-ray luminosity and spectral cutoff energy if CR in radiation-reaction limit from the current sheet is assumed. It has also been noted that sychrotro-curvature radiation provides a better description of pulsar hard X-ray to γ-ray spectra than treating SR and CR as separate processes [38, 44]. Modeling of the energy-dependent light curves and phase-resolved spectra could discriminate between the different competing emission mechanisms. A transition from SR or CR to IC or SSC around 50 - 100 GeV to explain the VHE emission observed from Vela, Geminga and B1706-44 would show a change in the P1/P2 ratio decrease with energy, although models have yet to demonstrate that SR can account for this trend observed by *Fermi*. If the GeV to VHE emission from these pulsars is pure CR [35], the P1/P2 trend should continue to the highest energy. Observations of the Crab have shown transitions between soft and hard X-ray light curve P1/P2 trends [45], indicating a change in emission mechanism. Such studies should be a future focus of both VHE observations and modeling.

It also has been noted that the issue of the GeV radiation mechanism can be resolved by measuring the polarization of the emission above 50 MeV [46]. In the case of CR, the predicted degree of linear polarization will be much higher than that of SR or ICS and the position angle of CR will be orthogonal to that of the lower-energy SR. A stronger indication that CR is the GeV radiation mechanism will come from detection of pulsed emission above 10 TeV and a measurement of a cutoff in such a component, requiring particles with Lorentz factors of at least 2×10^7. For particles with this energy in the current sheet of an FF magnetosphere, whose radii of curvature are now well established, the CR loss rate will greatly exceed that of SR. However, in models invoking Doppler boosting of SR, the cutoff of the VHE component will be related to the wind velocity rather than to the particle energy, which could vary between different pulsars. On the other hand, the current sheet models invoking radiation-reaction limited particle acceleration predict similar particle energies and spectral cutoff energies around 20-30 TeV for different pulsars [23]. Thus, measurement of VHE spectral cutoffs can provide strong discriminants and are likely to come from air Cherenkov telescopes within the next few years, providing a major advancement in understanding of particle acceleration by pulsars.

References

[1] A. A. Abdo, al., and Fermi LAT Collaboration, *Fermi Large Area Telescope Observations of the Vela Pulsar*, *ApJ* **696** (May, 2009) 1084–1093, [arXiv:0812.2960].

[2] A. A. Abdo, al., and Fermi LAT Collaboration, *A Population of Gamma-Ray Millisecond Pulsars Seen with the Fermi Large Area Telescope*, *Science* **325** (Aug., 2009) 848.

[3] A. A. Abdo, al., and Fermi LAT Collaboration, *Detection of 16 Gamma-Ray Pulsars Through Blind Frequency Searches Using the Fermi LAT*, *Science* **325** (Aug., 2009) 840, [arXiv:1009.0748].

[4] E. Aliu and MAGIC Collaboration, *Observation of Pulsed γ-Rays Above 25 GeV from the Crab Pulsar with MAGIC*, *Science* **322** (Nov., 2008) 1221, [arXiv:0809.2998].

[5] E. Aliu and VERITAS Coll., *Detection of Pulsed Gamma Rays Above 100 GeV from the Crab Pulsar*, *Science* **334** (Oct., 2011) 69, [arXiv:1108.3797].

[6] S. Ansoldi and MAGIC Collaboration, *Teraelectronvolt pulsed emission from the Crab Pulsar detected by MAGIC*, *Astronomy & Astrophysics* **585** (Jan., 2016) A133, [arXiv:1510.07048].

[7] H. Abdalla and H.E.S.S. Collaboration, *First ground-based measurement of sub-20 GeV to 100 GeV γ-Rays from the Vela pulsar with H.E.S.S. II*, *Astronomy & Astrophysics* **620** (Dec., 2018) A66, [arXiv:1807.01302].

[8] M. Spir-Jacob, A. Djannati-Ataï, L. Mohrmann, G. Giavitto, B. Khélifi, B. Rudak, C. Venter, and R. Zanin, *Detection of sub-100 GeV gamma-ray pulsations from PSR B1706-44 with H.E.S.S*, *arXiv e-prints* (Aug., 2019) arXiv:1908.06464, [arXiv:1908.06464].

[9] V. A. Acciari and MAGIC Collaboration, *Detection of the Geminga pulsar with MAGIC hints at a power-law tail emission beyond 15 GeV*, *A&A* **643** (2020) L14.

[10] J. Arons, *Pair creation above pulsar polar caps : geometrical structure and energetics of slot gaps.*, *ApJ* **266** (Mar., 1983) 215–241.

[11] A. G. Muslimov and A. K. Harding, *High-Altitude Particle Acceleration and Radiation in Pulsar Slot Gaps*, *ApJ* **606** (May, 2004) 1143–1153, [astro-ph/0402462].

[12] J. Dyks and B. Rudak, *Two-Pole Caustic Model for High-Energy Light Curves of Pulsars*, *ApJ* **598** (Dec., 2003) 1201–1206, [astro-ph/0303006].

[13] A. K. Harding, J. V. Stern, J. Dyks, and M. Frackowiak, *High-Altitude Emission from Pulsar Slot Gaps: The Crab Pulsar*, *ApJ* **680** (June, 2008) 1378–1393, [arXiv:0803.0699].

[14] Y. J. Du, G. J. Qiao, and W. Wang, *Radio-to-TeV Phase-resolved Emission from the Crab Pulsar: The Annular Gap Model*, *ApJ* **748** (Apr., 2012) 84, [arXiv:1202.1096].

[15] P. Goldreich and W. H. Julian, *Pulsar Electrodynamics*, *ApJ* **157** (Aug., 1969) 869.

[16] K. S. Cheng, C. Ho, and M. Ruderman, *Energetic Radiation from Rapidly Spinning Pulsars. I. Outer Magnetosphere Gaps*, *ApJ* **300** (Jan., 1986) 500.

[17] R. W. Romani and I. A. Yadigaroglu, *Gamma-Ray Pulsars: Emission Zones and Viewing Geometries*, *ApJ* **438** (Jan., 1995) 314, [astro-ph/9401045].

[18] A. J. Deutsch, *The electromagnetic field of an idealized star in rigid rotation in vacuo*, *Annales d'Astrophysique* **18** (Jan., 1955) 1.

[19] I. Contopoulos, D. Kazanas, and C. Fendt, *The Axisymmetric Pulsar Magnetosphere*, *ApJ* **511** (Jan., 1999) 351–358, [astro-ph/9903049].

[20] C. Kalapotharakos, D. Kazanas, A. Harding, and I. Contopoulos, *Toward a Realistic Pulsar Magnetosphere*, *ApJ* **749** (Apr., 2012) 2, [arXiv:1108.2138].

[21] J. Li, A. Spitkovsky, and A. Tchekhovskoy, *Resistive Solutions for Pulsar Magnetospheres*, *ApJ* **746** (Feb., 2012) 60, [arXiv:1107.0979].

[22] C. Kalapotharakos, A. K. Harding, and D. Kazanas, *Gamma-Ray Emission in Dissipative Pulsar Magnetospheres: From Theory to Fermi Observations*, *ApJ* **793** (Oct., 2014) 97, [arXiv:1310.3545].

[23] C. Kalapotharakos, G. Brambilla, A. Timokhin, A. K. Harding, and D. Kazanas, *Three-dimensional Kinetic Pulsar Magnetosphere Models: Connecting to Gamma-Ray Observations*, *ApJ* **857** (Apr., 2018) 44, [arXiv:1710.03170].

[24] A. A. Philippov and A. Spitkovsky, *Ab-initio Pulsar Magnetosphere: Particle Acceleration in Oblique Rotators and High-energy Emission Modeling*, *ApJ* **855** (Mar., 2018) 94, [arXiv:1707.04323].

[25] A. A. Philippov, B. Cerutti, A. Tchekhovskoy, and A. Spitkovsky, *Ab Initio Pulsar Magnetosphere: The Role of General Relativity*, *ApJL* **815** (Dec., 2015) L19, [arXiv:1510.01734].

[26] R. Hu and A. M. Beloborodov, *Axisymmetric pulsar magnetosphere revisited*, *arXiv e-prints* (Sept., 2021) arXiv:2109.03935, [arXiv:2109.03935].

[27] K. S. Cheng, C. Ho, and M. Ruderman, *Energetic Radiation from Rapidly Spinning Pulsars. II. VELA and Crab*, *ApJ* **300** (Jan., 1986) 522.

[28] K. Hirotani, *Gamma-Ray Emissions from Pulsars: Spectra of the TEV Fluxes from Outer Gap Accelerators*, *ApJ* **549** (Mar., 2001) 495–508, [astro-ph/0005421].

[29] J. Takata, H. K. Chang, and K. S. Cheng, *Polarization of High-Energy Emission from the Crab Pulsar*, *ApJ* **656** (Feb., 2007) 1044–1055, [astro-ph/0610348].

[30] J. Aleksić and MAGIC Collaboration, *Observations of the Crab Pulsar between 25 and 100 GeV with the MAGIC I Telescope*, *ApJ* **742** (Nov., 2011) 43, [arXiv:1108.5391].

[31] M. Lyutikov, *Pulsar high energy emission due to inverse Compton scattering*, *Nuclear Physics B Proceedings Supplements* **239** (June, 2013) 61–63.

[32] F. A. Aharonian, S. V. Bogovalov, and D. Khangulyan, *Abrupt acceleration of a 'cold' ultrarelativistic wind from the Crab pulsar*, *Solar Physics* **482** (Feb., 2012) 507–509.

[33] I. Mochol and J. Petri, *Very high energy emission as a probe of relativistic magnetic reconnection in pulsar winds.*, *MNRAS* **449** (Apr., 2015) L51–L55, [arXiv:1501.07123].

[34] A. K. Harding and C. Kalapotharakos, *Synchrotron Self-Compton Emission from the Crab and Other Pulsars*, *ApJ* **811** (Sept., 2015) 63, [arXiv:1508.06251].

[35] A. K. Harding, C. Venter, and C. Kalapotharakos, *Very-High-Energy Emission From Pulsars*, *arXiv e-prints* (Oct., 2021) arXiv:2110.09412, [arXiv:2110.09412].

[36] R. W. Romani, *Gamma-Ray Pulsars: Radiation Processes in the Outer Magnetosphere*, *ApJ* **470** (Oct., 1996) 469.

[37] Y. Wang, J. Takata, and K. S. Cheng, *Three-dimensional two-layer outer gap model: Fermi energy-dependent light curves of the Vela pulsar*, *MNRAS* **414** (July, 2011) 2664–2673, [arXiv:1102.4474].

[38] A. K. Harding, C. Kalapotharakos, M. Barnard, and C. Venter, *Multi-TeV Emission from the Vela Pulsar*, *ApJL* **869** (Dec., 2018) L18, [arXiv:1811.11157].

[39] M. Barnard, C. Venter, A. K. Harding, C. Kalapotharakos, and T. J. Johnson, *Probing the High-energy γ-ray Emission Mechanism in the Vela Pulsar via Phase-resolved Spectral and Energy-dependent Light Curve Modeling*, *arXiv e-prints* (Nov., 2021) arXiv:2111.03405, [arXiv:2111.03405].

[40] G. Brambilla, C. Kalapotharakos, A. N. Timokhin, A. K. Harding, and D. Kazanas, *Electron-Positron Pair Flow and Current Composition in the Pulsar Magnetosphere*, *ApJ* **858** (May, 2018) 81, [arXiv:1710.03536].

[41] B. Cerutti, A. A. Philippov, and A. Spitkovsky, *Modelling high-energy pulsar light curves from first principles*, *MNRAS* **457** (Apr., 2016) 2401–2414, [arXiv:1511.01785].

[42] M. Lyutikov, N. Otte, and A. McCann, *The Very High Energy Emission from Pulsars: A Case for Inverse Compton Scattering*, *ApJ* **754** (July, 2012) 33, [arXiv:1108.3824].

[43] C. Kalapotharakos, A. K. Harding, D. Kazanas, and Z. Wadiasingh, *A Fundamental Plane for Gamma-Ray Pulsars*, *ApJL* **883** (Sept., 2019) L4, [arXiv:1904.01765].

[44] D. F. Torres, D. Viganò, F. Coti Zelati, and J. Li, *Synchrocurvature modelling of the multifrequency non-thermal emission of pulsars*, *MNRAS* **489** (Nov., 2019) 5494–5512, [arXiv:1908.11574].

[45] L. Kuiper, W. Hermsen, G. Cusumano, R. Diehl, V. Schönfelder, A. Strong, K. Bennett, and M. L. McConnell, *The Crab pulsar in the 0.75-30 MeV range as seen by CGRO COMPTEL. A coherent high-energy picture from soft X-rays up to high-energy gamma-rays*, *A&A* **378** (Nov., 2001) 918–935, [astro-ph/0109200].

[46] A. K. Harding and C. Kalapotharakos, *Multiwavelength Polarization of Rotation-powered Pulsars*, *ApJ* **840** (May, 2017) 73, [arXiv:1704.06183].